***Manuscript refereed by Dr Iñigo Agote (TECNALIA, Spain)***

# Binder Jetting as Complementary Technology to Metal Injection Molding: influence of HIP on microstructure and mechanical properties

Simone Herzog[1] S.Herzog@iwm.rwth-aachen.de, Anke Kaletsch[1] A.Kaletsch@iwm.rwth-aachen.de, Sebastian Riehm[1] S.Riehm@iwm.rwth-aachen.de, Ekaterina Andreeva[2] ekaterina.andreeva@ifam.fraunhofer.de, Thomas Hartwig[2] thomas.hartwig@ifam.fraunhofer.de, Christoph Broeckmann[1] C.Broeckmann@ifam.fraunhofer.de

[1] Institute for Materials Applications in Mechanical Engineering, RWTH Aachen University, Augustinerbach 4, 52062 Aachen, Germany

[2] Fraunhofer Institute for Manufacturing Technology and Advanced Materials IFAM, Wiener Straße 12, 28359 Bremen, Germany

## Abstract

Binder jetting (BJT) is a binder-based additive manufacturing technology and is especially suited for the shaping of complex parts in small batch series. Further processing (debinding and sintering) is similar to metal injection molding (MIM). For this reason, BJT can beneficially complement MIM, which is an established technology for large-scale production of small-sized, complex net-shape parts.

This study compares the performance of BJT parts made of stainless maraging steel AISI 630 (17-4PH) to standard values of MIM parts. Investigations include light microscopy, scanning electron microscopy, hardness and roughness measurements as well as tensile and impact testing. Special attention is paid to the anisotropic properties of BJT specimen. We show that HIP can improve the mechanical properties of BJT parts while decreasing their anisotropic nature. However, properties fulfilling minimum standard requirements are obtained also without HIP what may be sufficient for many applications.

## Keywords

Metal Binder Jetting, Metal Injection Molding, Additive Manufacturing, Anisotropy, impact test

## 1 Introduction

Metal injection molding (MIM) is an established powder metallurgy process for complex-shaped components in large-scale production. MIM is a thermoplastic process, where metal powder and binder are mixed, granulated and injected into a mold at elevated temperatures. The obtained green body has to be debindered and sintered afterwards. Advantageously, the geometry after sintering does not necessitate any mechanical post-machining. However, every component geometry requires its own injection mold. The shapes have to be optimized in a complex manner in order to manufacture netshape components. MIM injection molds are expensive in production, which makes MIM inflexible and economical only for large-scale production.

For small-scale production of powder metallurgical components with complex geometries in high quality, additive manufacturing (AM) processes are available. One AM process that has much in common with MIM is 3D printing using binder jetting technology (BJT). BJT has a higher production rate than beam-based AM technologies such as laser powder-bed fusion (LPBF) or electron-beam melting (EBM) [1]. In BJT, a binder is selectively injected into a powder bed with a printhead. This is done layer by layer until the desired geometry is built. The part consisting of cemented powder particles is called green part. Green parts need to be removed from the powder bed, debindered and sintered. To ensure the reliable use of BJT components and provide a suitable complement to MIM for small batches, some challenges have to be overcome first. Up to now, the process stability, reproducibility and mechanical performance are not ensured [2]. Although several studies provide values for the tensile strength, yield strength, elongation and hardness of AISI 316L [3–5] less information are available on AISI 630 [6]. Supplier specifications do not consider the direction-dependent properties, and post processing conditions are not specified [7, 8]. Until now, HIP was used for post densification of sintered BJT copper parts [9] to improve the mechanical properties and for sintering of pre-sintered samples without pore closure [10].

This article presents a study on the performance of AISI 630 BJT components in comparison to AISI 630 MIM components. The aim is to qualify BJT as a complementary technology to MIM for small batch production or prototypes and to provide a data set to decide whether HIP processing is necessary for a distinct application.

© European Powder Metallurgy Association (EPMA)

## 2 Materials and Methods

Corrosion-resistant and martensitic precipitation-hardening steel AISI 630 (Werkstoff-Nr. 1.4548, DIN X5CrNiCuNb17-4-4, 17-4PH©) was used with the chemical composition given in **Table 1**.

**Table 1:** Chemical compositions of the AISI 630 powder (%-wt) according to supplier´s specifications.

| C | Cr | Ni | Cu | Nb | Mo | Mn | O | N | Si | P | S | Fe |
|---|---|---|---|---|---|---|---|---|---|---|---|---|
| 0.018 | 16.6 | 4.2 | 4.0 | 0.32 | <0.03 | 0.54 | 0.06 | <0.1 | 0.4 | 0.04 | <0.01 | Bal. |

Typical MIM powder was selected for this study to investigate if MIM manufacturers have to buy special binder jetting powders or can flexibly work with their existing MIM powders. The fine powder with average nominal particle size D90 < 22µm was obtained by gas atomization. It consists of spherical particles with few satellites (**Figure 1a, b**). Parameters for specimen fabrication by BJT, sintering, hot isostatic post-densification and heat treatment are summarized in **Table 2.**

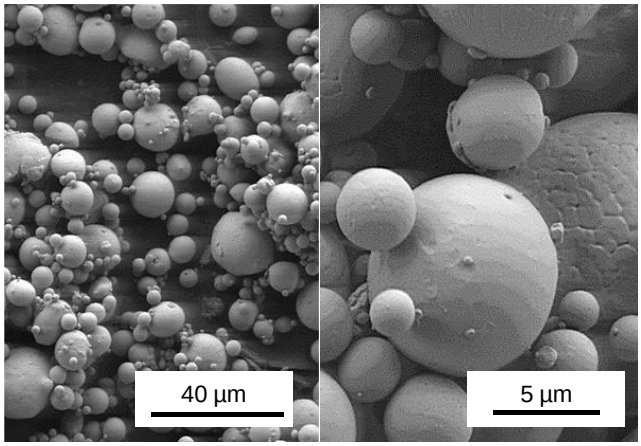



**Figure 1:** SEM images of AISI 630 powder particles

**Table 2:** BJT/post processing parameters

| | |
|---|---|
| BJT | • BJT unit: ExOne Innovent+<br>• Layer thickness: 40 µm B<br>• Binder: IFAM development<br>• Binder saturation: 65%<br>• Scale factor: 119% (x,y); 122% (z) |
| Sinter-ing | Thermal debinding + sintering in $H_2$<br>• 2K/min to 300°C (60 min)<br>• 2K/min to 650°C (60 min)<br>• 5K/min to 1370°C (120 min)<br>• 10K/min to RT |
| HIP | $T_{HIP}$=1150°C, $p_{HIP}$=100MPa und $t_{dwell}$ =3h |
| HT | H900 heat treatment (ASTM A564)<br>• Annealing in vacuum at 1020°C (30min)<br>• Quenching in $N_2$<br>• Age hardening at 480 °C in air (1h) |

A scale factor of 119% for x- and y-direction and 122% in z-direction was applied to the desired geometry of the specimen to compensate for the anisotropic sinter shrinkage. The printhead movement is parallel to the x-direction, the powder coater and roller move parallel to the y-direction, and the build platform is lowered in z-direction, see **Figure 2a**). In this coordinate system small (10 x 10 x 10 mm³) and big (30 x 30 x 30 mm³) cubes were built for microstructure, hardness and roughness analyses.

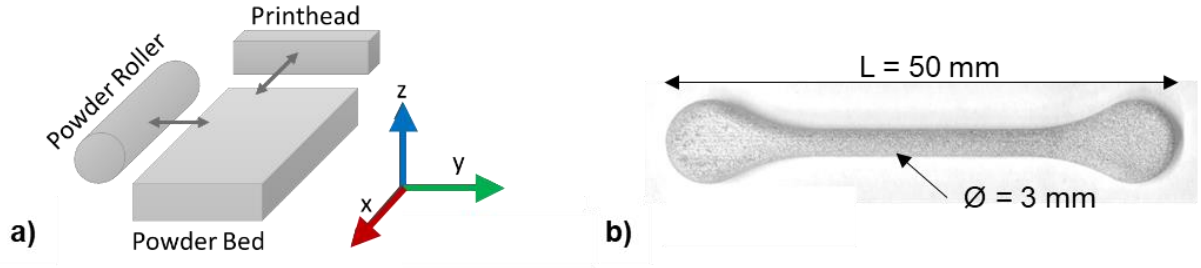



**Figure 2:** a) Schematic figure to define the coordinate system of BJT, and b) sample geometry of a sintered, down-scaled tensile specimen.

Flat tensile samples oriented in z-direction could not be manufactured as recommend in the ISO 2740 (shape B) with the total length of 90 mm due to building chamber limitations. The standard geometry was down-scaled to the dimensions shown in **Figure 2b.** 40 specimens were obtained in each direction (length L parallel to the x-, y- and z- direction). Each 20 specimens were tested in the heat-treated condition (HT) and in HIP post-densified and age hardened condition (HIP+HT), respectively. No surface finishing was applied. Impact bending specimens measuring 5 x 10 x 50 mm³ were also tested in the HT and HIP+HT condition and depending on the building chamber orientation. The length of the specimens was parallel to the three construction directions. In total 14 specimens oriented in x-direction, 89 specimens oriented in y-direction, and 31 specimens oriented in z-direction were

© European Powder Metallurgy Association (EPMA)

fabricated. No notches were inserted and the surface was not mechanically reworked. Testing was according to MPIF Standard 59.

Microstructural analyses were operated with light microscopy (LM) on polished cross-sections of small cubes, both chemically etched and non-etched. V2A etching agent was used at 60 °C for 75 seconds. Porosity analysis, as well as analysis of delta-ferrite content was determined by image analysis in ImageJ [11]. Vickers hardness was measured on as-sintered and heat-treated big cubes according to DIN EN ISO 6507-1:2018. Surface roughness was measured with a Taylor-Hobson PRECISION machine according to DIN EN ISO 4288:1998 on sintered big cubes. On each surface area of the cube, six test lines with a length of 20 mm each were measured. This corresponds to 36 measurements per cube in total. To investigate the influence of building direction and geometry, one cube was built up standing on a surface area and one cube was built up standing on the tip.

Tensile bones were tested at room temperature on a Zwick/Roell ZMART.PRO testing machine. Impact bending specimens were tested at different temperatures in the range -196°C to +400 °C (2 mm fin radius 2 mm, 150 J working capacity). Samples were tested within 3 seconds after leaving the temperature control medium. The distinct temperatures and used media were: -196°C (liquid nitrogen), -72°C (pure ethanol + dry ice), -21°C (100g $H2O_{(s)}$ + 33g NaCl), 0°C ($H_2O_{(s)}$ + $H_2O_{(l)}$), 24.5 °C (room temperature), and 60°C, 100°C, 200°C, 300°C, 400°C (chamber furnace). Since significantly more specimens were available for the series along the y-direction, mostly five measurements per temperature level were carried out in y-series, two measurements per temperature level for the z-series and only one measurement per temperature level for the x-series.

## 3 Results and discussion

**Figure 3** shows the martensitic-ferritic microstructure of AISI 630 after sintering. In the unetched cross-section in **Figure 3a** regularly distributed pores are found. Some of these pores are elongated in the x-y building plane, which is perpendicular to the z-building direction. The average density determined by image analysis and Archimedes' method is between 95% and 97%. **Figure 3b** and **3c** depict the phase composition after etching. The amount of δ-ferrite, determined by image analysis, is relatively high at 24%-vol. but depends on the high sintering temperature [11]. However, the δ-ferrite content described in literature [11–13] for sintering temperatures between 1350°C – 1380°C is in the range of 8 – 10%-vol for MIM samples. In [14], 7%-vol δ-ferrite and a density above 98% were obtained for sintered BJT samples. One explanation for the high δ-ferrite content in our samples might be the different residual carbon content after debinding. Low carbon contents increase the δ-ferrite content significantly [15].

Pore ribbons showing locally higher porosity can be observed in **Figure 3b** (marked with red lines). These ribbons of increased porosity are regularly distributed in the microstructure and have in this cross-section plane a lateral width of around 500 µm. They are observed due to a small angular offset (<1°) between the preparation plane and the x-y building plane. In microsections parallel to the x-z-plane (for example **Figure 3a**) such pore ribbons can be hardly observed. However, CT-measurements of green bodies showed a layer-wise stacking of high- and low-density areas. We assume that the periodic binder injection/penetration leads to an anisotropic distribution of binder or particles in the green parts. Whether the increased porosity occurs at the boundary between the powder bed layers or at the penetration limit of the binder remains open. Nevertheless, the anisotropic green density can result in an anisotropic pore distribution in the sintered material which is linked to anisotropic mechanical properties.

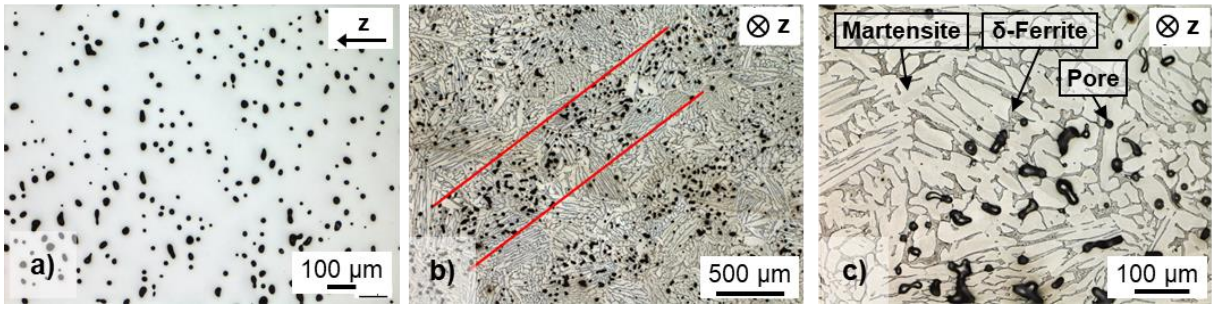



**Figure 1:** Microstructure after sintering a) and etching b,c). Distinct porous areas in the as-sintered condition are marked with red lines.

HIP was capable to reduce the porosity significantly, as demonstrated by the unetched microstructure image in **Figure 4a)**. Some pores with ferret diameters up to 5 µm were detected in high magnification. Precipitation-hardening without prior HIP densification has no influence on the porosity, but the δ-Ferrite content seems to be reduced, see **Figure 4b** (in comparison to **Figure 3c**). Until now

© European Powder Metallurgy Association (EPMA)

we could neither quantitatively confirm this by image analysis (due to similar colour of δ-Ferrite and Martensite) nor by XRD (due to overlapping pattern). The significant differences in pore size were determined and are visualized in **Figure 4b** were the ferret pore diameter $d_{90}$ was reduced from 30 µm to 3 µm by HIP.

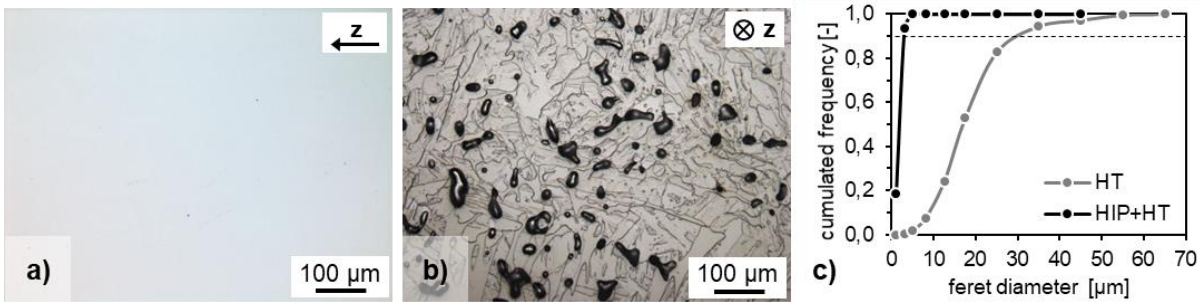



**Figure 4:** Microstructure in the conditions a) HIP+HT and b) HT; c) pore size distributions

The lowest roughness Ra measured **(Figure 5)** is in the range of 2.5 µm, but on the same surface also 3 to 4 µm have been measured. In general, a high scattering is observed giving a hint that depowdering prior to debinding and sintering might be improved. The overhanging structures in **Figure 5b** do not reach the roughness of 2.5 µm, but are not significantly worse than the vertically and the horizontally surfaces. The surface roughness is approximately three times higher than to the roughness determined at typical MIM components (Ra = 0,97 ± 0,20 and Rz= 4,83 ± 1,09).

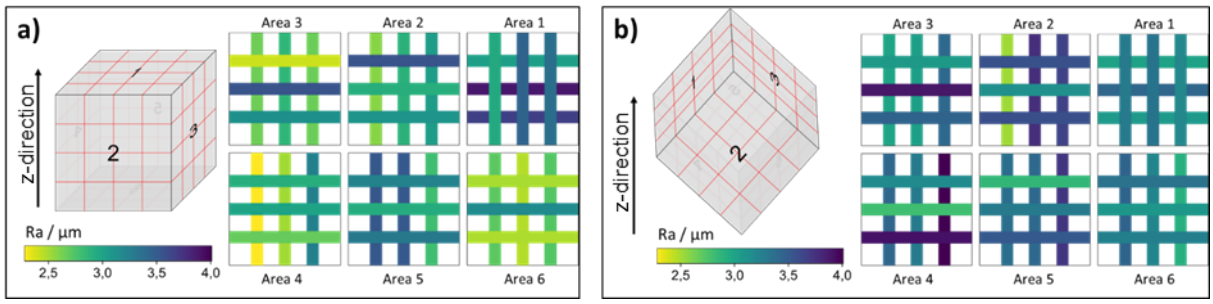



**Figure 5:** Surface roughness of sintered cubes with different building directions: a) build-up standing on a surface area, b) build-up standing on a vertice

Hardness indents on the distinct surface areas show a statistical and not a direction-dependent scatter between 230 and 290 HV10 (**Figure 6**). After age-hardening a hardness of 360 HV10 was measured and the typical MIM reference value of 325 HV10 is fulfilled. This observation strengthens the assumption that the H900 treatment adjusts the δ-ferrite content besides the precipitation hardening. The reduced δ-ferrite content increases at the same time the content of martensite.

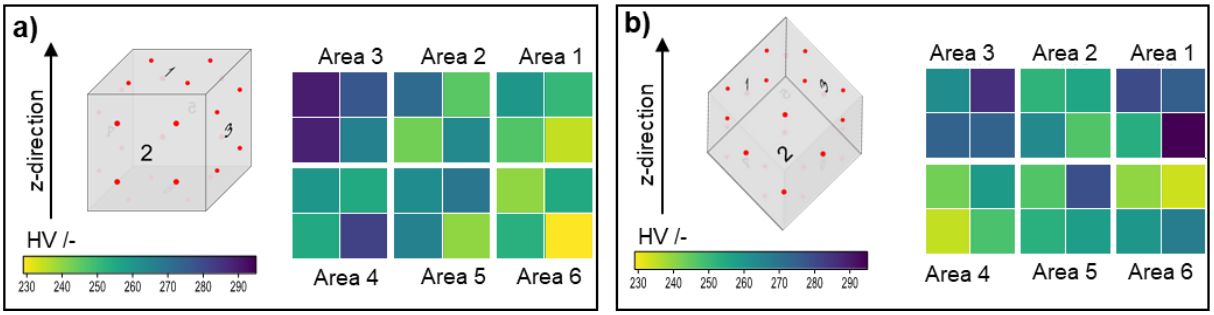



**Figure 6:** Hardness HV10 of sintered cubes with different building directions: a) built-up standing on a surface area, b) built-up standing on a vertice.

The anisotropic porosity of the BJT samples, shown in **Figure 3,** has a significant influence on the mechanical properties determined in tensile testing. Results in **Figure 7** are presented as box-plots**.** The dotted line shows the typical MPIF 35 standard [16] for MIM samples after H900 heat treatment.
For the yield strength, a distinct anisotropy is visible. The values for the samples built in x- and y-direction differ significantly from the values of the z-samples. The samples built in x- and y-direction fit the standard while samples built in z- direction did not reach the required proof stress. Regarding ultimate tensile strength, the behaviour is ambiguous, but the differences between x- and y-direction are increased. Post densification with HIP improves the yield strength and tensile strength, and the

© European Powder Metallurgy Association (EPMA)

differences between the different build directions decrease. After HIP even the worse outliers fulfil the requirement of the MIM standard. However, a slightly lower average value for the samples built in z-direction is still visible in tensile testing. Additionally, an increase in scattering is visible after HIP. Usually, the opposite can be expected. It is possible that a small number of samples was not totally densified during HIP due to local areas with open porosity. As mentioned before, the relative density of the samples prior to HIP was around 95%. This value is considered as threshold for the transition to closed porosity, which is required for HIP post densification. This hypothesis is not validated yet and needs further investigation, like microstructure analysis of all tested samples. Nevertheless, it is proved that a HIP post-treatment results in a reliable improvement of the mechanical strength. This is only possible if the majority of porosity within the BJT samples can be characterized as „closed porosity“.

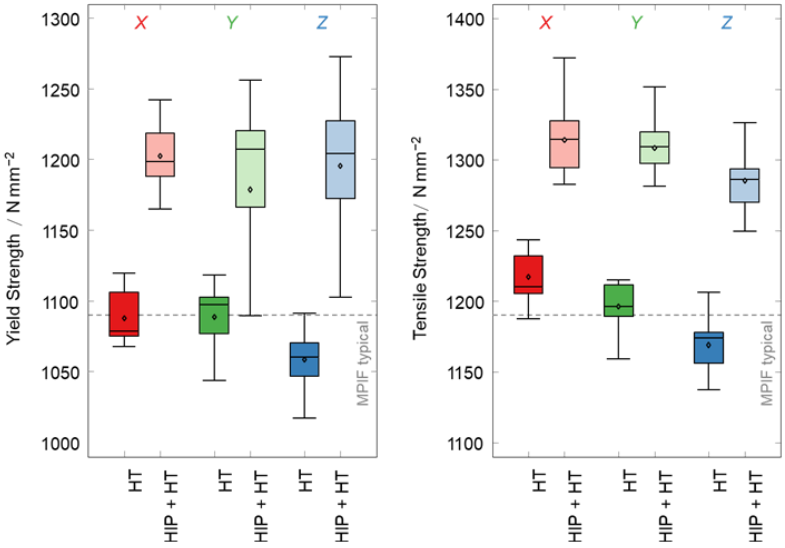



**Figure 7**: Results of tensile tests of specimens built in different directions in the HT and HIP+HT condition

Similar trends as observed during tensile testing are apparent in impact testing, see **Figure 8**. For quantitative evaluation of the data points, curve fitting, using the logistic distribution function

$$K_2 = \frac{C_1}{1 + e^{-C_2 \cdot (T - C_3)}} + C_4$$

was applied. The fitting parameters describe the toughness-temperature function as follows: $C_1$ - impact toughness in the upper shelf, $C_2$ - curvature of the flank, $C_3$ - transition temperature, $C_4$ – impact toughness in the lower shelf.

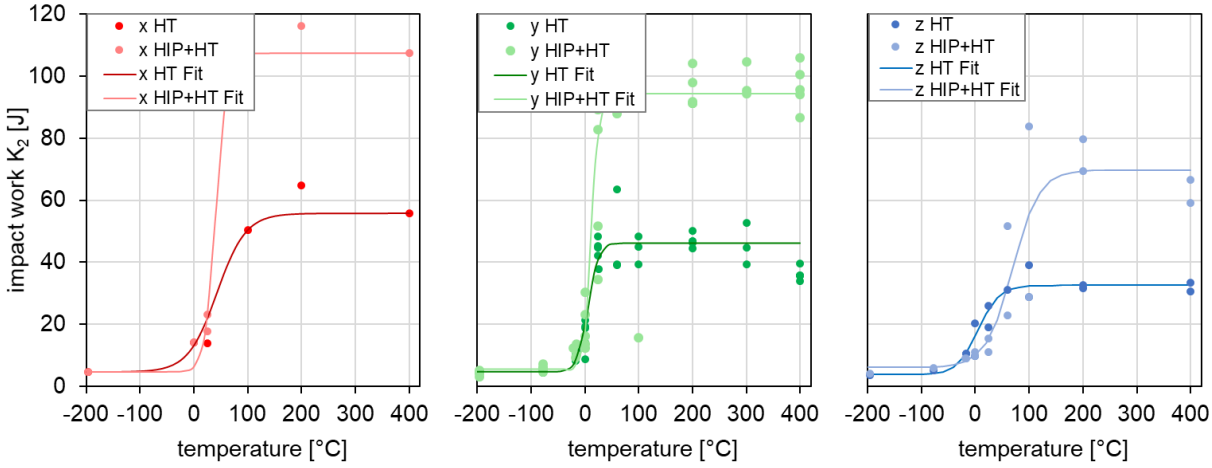



**Figure 8:** Results of directional impact tests in the HT and HIP+HT condition.

The results indicate that building direction and the HIP post-treatment have a significant effect on the height of the upper shelf and a slight effect on the ductile-to-brittle transition temperature. Prior to HIP, the highest toughness (56 J) has been determined in the sample batch built in x-direction, followed by the y-direction with 46 J. In z-direction the upper shelf could be identified at 33 J. The same ranking applies to the specimens after HIP post-treatment. In general, HIP doubles the toughness measured under ductile fracture (x: 56 → 107 J, y: 46 → 94 J, z: 33 → 77 J). At 400 °C, a decreased toughness occurs, compared to the values at 300 °C. Note, that this was not considered in the fit for simplicity. It is well known from duplex- as well as from maraging steels, that precipitation of intermetallic phases reduces the impact toughness at testing temperatures higher than 350°C. No sample series meets the requirements of the MPIF standard (135 J at room temperature). This is attributed to general level of

© European Powder Metallurgy Association (EPMA)

the upper shelf and the low transition temperature $C_3$ between 7 and 69 °C. A very low toughness of 14 ± 8 J for pressed, sintered and H900 hardened AISI 630 was also obtained in literature [17].

## 4 Conclusion and outlook

This work demonstrated that binder jetting of AISI 630 results in highly anisotropic microstructure and mechanical properties. The elastic limit ($R_{p0.2}$), ultimate tensile strength (UTS) and impact toughness strongly depend on the direction of loading with respect to the building direction. Minimum and even typical MIM properties (except outliners in yield strength) could be achieved even without HIP. Nevertheless, it was concluded that the mean porosity prior to HIP was in the transition range of open- to closed porosity, leaving surface near regions of open porosity in the samples, that could not be closed during HIP. This might be the reason for high and untypical scatter of material properties after HIP. **Table 2** gives an overview of the direction independent mean values and standard deviations, which may be helpful for design engineers.

**Table 2:** Comparison of obtained properties with BJT processing in comparison to MIM reference values of MPIF Standard 35 at room temperature. BJT properties are mean values of the directional properties with standard deviation. Note: * own measurement of MIM component, ** minimal/typical value.

| property | unit | BJT | | | MIM |
|---|---|---|---|---|---|
| | | sintered | HT | HIP + HT | |
| HV10 | [-] | 260 | 360 | | 325 |
| Roughness Ra | [µm] | 3.32 ± 0.32 | | | 0.97 ± 0.20* |
| Roughness Rz | [µm] | 16.09 ± 1.35 | | | 4.83 ± 1.09* |
| Yield strength $R_{p0.2}$ | [MPa] | | 1078 ± 24 | 1191 ± 47 | 970/1090** |
| Tensile strength UTS | [MPa] | | 1191 ± 26 | 1303 ± 23 | 1070/1190** |
| Impact toughness | [J] | | 27 ± 12 | 34 ± 25 | 136 |

## 5 Acknowledgement

This work was funded via AiF (project number 19733 N of FSV e. V. Hagen) within the context of IGF by the Federal Ministry of Economics and Energy thanks to a resolution of the German Bundestag.

Bundesministerium für Wirtschaft und Energie

## 6 References

[1] P.K. Gokuldoss, S. Kolla, J. Eckert, Materials 10 (2017)
[2] M. Li, W. Du, A. Elwany, Z. Pei, C. Ma, J Manuf Sci Eng 142 (2020) 1917
[3] U. Attia, D. Adamuks, Proceedings of EuroPM2019; Maastricht 2019
[4] B. Barthel, S. Hein, F. Petzoldt, Proceedings of EuroPM2019; Maastricht 2019
[5] S. Mirzababaei, S. Pasebani, JMMP 3 (2019) 82
[6] E. Carreño-Morelli, S. Martinerie, L. Mucks, B. Cardis, MSF 591-593 (2008) 374–379
[7] Digital Metal, DIGITAL METAL®Materials for 3D Printing, https://digitalmetal.tech/materials
[8] ExOne, Metal 3D Printing Materials and Binders of ExOne, https://www.exone.com/en-US/3d-printing-materials-and-binders/metal-materials-binders
[9] A. Kumar, Y. Bai, A. Eklund, C.B. Williams, Procedia Manufacturing 10 (2017) 935–944
[10] K. Inaekyan, V. Paserin, I. Bailon-Poujol, V. Brailovski, Proceedings AMPM Conf. Boston (2016)
[11] R. German, PIM International 12(2) (2018) 47–76
[12] K. Murray, A.J. Coleman, T.A. Tingskog, D.T. Whychell, Int J Powder Metall 2011
[13] H.Ö. Gülsoy, S. Özbek, T. Baykara, Powder Metall 50 (2007) 120–126
[14] A. Lores, N. Azurmendi, I. Agote, U. Andrés, Proceedings of EuroPM2020; online 2020
[15] Y. Wu, R.M. German, D. Blaine, B. Marx, C. Schlaefer, J Mater Sci 37 (2002) 3573–3583
[16] MPIF, Materials Standards for Metal Injection Molded Parts: MPIF Standard 35 2016
[17] P. Suri, B.P. Smarslok, R.M. German, Powder Metall 49 (2006) 40–47

© European Powder Metallurgy Association (EPMA)